

# Hearing What You Cannot See: Acoustic Detection Around Corners

Yannick Schulz<sup>\*1</sup>

Avinash Kini Mattar<sup>\*1</sup>

Thomas M. Hehn<sup>1</sup>

Julian F. P. Kooij<sup>1</sup>

**Abstract**—This work proposes to use passive acoustic perception as an additional sensing modality for intelligent vehicles. We demonstrate that approaching vehicles behind blind corners can be detected by sound before such vehicles enter in line-of-sight. We have equipped a hybrid Prius research vehicle with a roof-mounted microphone array, and show on data collected with this sensor setup that wall reflections provide information on the presence and direction of approaching vehicles. A novel method is presented to classify if and from what direction a vehicle is approaching before it is visible, using as input Direction-of-Arrival features that can be efficiently computed from the streaming microphone array data. Since the ego-vehicle position within the local geometry affects the perceived patterns, we systematically study several locations and acoustic environments, and investigate generalization across these environments. With a static ego-vehicle, an accuracy of 92% is achieved on the hidden vehicle classification task, and approaching vehicles are on average detected correctly 2.25 seconds in advance. By stochastic exploring configurations using fewer microphones, we find that on par performance can be achieved with only 7 out of 56 available positions in the array. Finally, we demonstrate positive results on acoustic detection while the vehicle is driving, and study failure cases to identify future research directions.

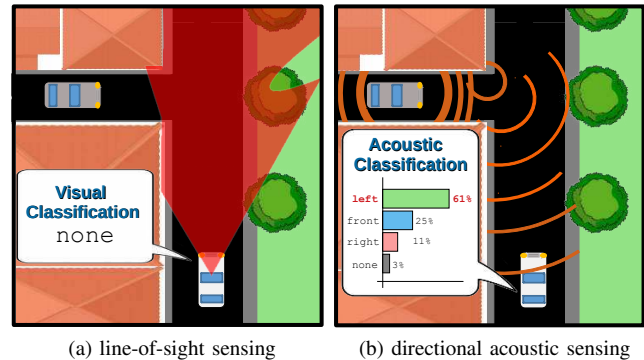
## I. INTRODUCTION

Highly automated and self-driving vehicles currently rely on three main sensors to identify visible objects, namely camera, lidar, and radar. Each sensor has its own advantages and disadvantages, thus multiple sensing modalities are used to increase robustness or to perform complementing tasks. However, the capabilities of these conventional sensors can be limited in urban environments when sight is obstructed by narrow streets, trees, parked vehicles, and other traffic. Approaching road users may therefore remain undetected by the main sensors, resulting in dangerous situations and last-moment emergency maneuvers [1]. While future V2X might help to reduce this problem, creating a robust omnipresent communication layer is still an open problem [2], and excludes road users without wireless capabilities.

Acoustic perception does not rely on line-of-sight, and can provide a wide range of complementary and important cues on nearby traffic: There are salient sounds with specified meanings, e.g. sirens, car horns, and reverse driving warning beeps of trucks, but also inadvertent sounds, such as tire-road contact and engine sounds of cars, buses, mopeds, cyclists.

In this work, we propose to use multiple cheap microphones to capture traffic sound as an additional sensing modality for early detection of approaching vehicles

<sup>\*</sup>) Shared first authors. 1) All authors are with the Intelligent Vehicles Group, TU Delft, The Netherlands. Primary contact: J.F.P.Kooij@tudelft.nl



(c) Sound localization with a vehicle-mounted microphone array detects the wall reflection of an approaching vehicle behind a corner before it appears

Fig. 1. When an intelligent vehicle approaches a blind corner, (a) traditional line-of-sight sensors cannot determine if the corner is safe to pass until the vehicle is much closer, while (b) acoustic cues can provide early warnings of an approaching vehicle. Directional information confirms that the sound comes from around corner, and not a different source. (c) shows this effect using real-time beamforming in real outdoor conditions.

behind blind corners. Crucially, our data-driven approach classifies acoustic reflection patterns to identify dangerous situations in urban settings with occlusions and alleys. This can provide early warnings before conventional line-of-sight sensing detects the approaching traffic, see Figure 1. While a vehicle should always exit a narrow street or walled garage cautiously, such early warning would reduce the need for last-moment emergency braking.

## II. RELATED WORKS

We here review the most relevant applications and methods for our approach, before listing this paper's contributions.

In the automotive domain, acoustics are typically found in active ultrasonic near-range sensing [3]. Although acoustic cues are known to be crucial for traffic awareness by pedestrians and cyclist [4], only few works have explored passive acoustic sensing as a sensor for Intelligent Vehicles (IV). [5], [6], [7] focus on detection and tracking in direct line-of-sight. [8], [9] address detection behind corners from a static observer. [8] only show experiments without directional

estimation. [9] tries to accurately model wave refractions, but experiments in an artificial lab setup show limited success. Both [8], [9] rely on strong modeling assumptions, ignoring that other informative patterns could be present in the acoustic data.

Acoustic traffic perception is furthermore used for roadside traffic monitoring, e.g. to counting vehicles and estimating traffic density [10], [11]. It is important to note that Electric Vehicles (EVs) may reduce overall traffic noise, though [12] shows that at 20-30km/h the noise levels for EV and internal combustion vehicles are already similar due to tire-road contact. The study in [13] finds that at lower speeds the difference is only about 4-5 dB, while many EVs also suffer from audible narrow peaks in the spectrum. Since low speed EVs may impact acoustic perception of human traffic participants [4], legal minimum sound requirements are being proposed [14], [15].

Outside IV, acoustic sensing is an active research topic in domains such as surveillance [16] and robotics [17], e.g. to localizing and separating dominant sound sources [18], [19]. While mobile robotic platforms in outdoor environments may suffer from vibrations and wind, various works have demonstrated detection and localization of salient sounds on moving drones [20] and wheeled platforms [21], [6]. Direction-of-Arrival estimation is a key task for sound source localization, and over the past decades many methods have been proposed, popular choices [22] include Steered-Response Power Phase Transform (SRP-PHAT) [23], which is well-suited for reverberant environments with possibly distant unknown sound sources, and MULTiple SIGNAL Classification (MUSIC) [24], which performs subspace analysis of the received signal covariance to identify uncorrelated source signals. Intuitively, such signal processing techniques triangulate sources by comparing differences in signal arrival time, and generate spatial distributions of source locations through beamforming. Still, in urban settings nearby walls, corners and surfaces distort sound signals through reflections and diffractions [25]. Accounting for such distortions can improve localization [21], [26].

Recently, data-driven methods have shown promising results in challenging real-world conditions for various acoustic tasks. For instance, learned sound models assist monaural source separation [27], and source localization from direction-dependent attenuations by fixed structures [28]. Increasingly, deep learning is used for audio classification [29], [30], localization [19], and even sound wave generation [31]. Analogous to our work, [32] presents a first deep learning method for non-line-of-sight sensing but with automotive radar rather than sound. While the effect of occlusions on sensors measurements is difficult to model [9], learning these from data thus appears a good alternative.

This paper provides the following contributions:

- 1) A novel perception method for intelligent vehicles is proposed, which detects approaching vehicles behind blind corners using only vehicle-mounted microphones, before line-of-sight detection is feasible. The task is cast as a multi-class classification problem to

identify if and from what corner a vehicle is approaching. We demonstrate that good results can already be obtained using robust and well known Direction-of-Arrival features as the input to our classifier, even without deep learning a feature extractor on large amounts of data.

- 2) We present a new demonstrator vehicle setup with a front-facing microphone array, which can be used for synchronized data collection with other common vehicle sensors. The prototype array will be used to study the impact of array design choices (e.g. number of microphones), and facilitates experimentation with future acoustic perception tasks, for which we will show a few potential use cases.
- 3) We collected a new audio-visual dataset with our research vehicle in real-world urban environments. Using this data we investigate the impact on accuracy of our task for various conditions, such as different locations and acoustic environments, moving versus static ego-vehicle, and the number of microphones.

### III. APPROACH

In this section, we first provide details of our novel vehicle sensor setup, and then describe our occluded vehicle detection method that we developed on this platform.

#### A. Acoustic perception research vehicle

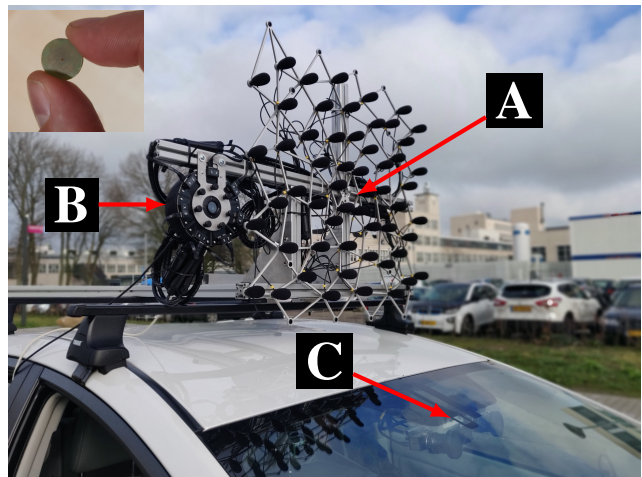


Fig. 2. Sensor setup of our test vehicle. A: Center of the 56 MEMS acoustic array. B: signal processing unit. C: front camera behind windshield. Inset: the diameter of a single MEMS microphone is only 12mm.

We have mounted a custom microphone array on the roof rack of our research vehicle [33], a hybrid electric Toyota Prius. The microphone array hardware consists of 56 ADMP441 MEMS microphones, support data acquisition at 48 kHz sample rate, 24 bits resolution, synchronous sampling, and was bought from *CAE Software & Systems GmbH* with a metal frame that distributes the microphones almost uniformly but irregularly in a  $0.8m \times 0.7m$  square. The general purpose layout was designed by the company through stochastic optimization to have large variance in



(a) Stroller at a distance (b) Electric scooter (c) Scooter overtaking (d) Car passing by (e) Oncoming car

Fig. 3. Qualitative examples of 2D Direction-of-Arrival estimation overlaid on the camera image (zoomed). (a): Stroller wheels are picked up even at a distance. (b), (c): Both conventional and more quiet electric scooters are detected. (d): The loudest sound of a passing vehicle is typically the road contact of the individual tires. (e): Even when the ego-vehicle drives at  $\sim 30$  km/h, oncoming moving vehicles are still registered as salient sources.

inter-microphone distances and serve a wide range of acoustic imaging tasks. The center of the microphone array (see Figure 2) is about 1.78m above the ground, and 0.54m above and 0.50m behind the used front camera.

The vehicle is also equipped with cameras (and other sensors, not used in this work) for data collection and processing. A signal processing unit receives the analog microphone signals, and sends the data to the PC through Ethernet running a custom software interface for the Robot Operating System (ROS). As depicted in the inset of the Figure 2, the microphones themselves are only 12mm wide and cost only about US\$1. In the future, the array can be rearranged with fewer microphones and placed at different locations around the vehicle rather than on top, and integrated in a smaller form factor. Still, the large array has research benefits to investigate the impact on the number of microphones, and the 2D planar microphone arrangement provides both horizontal and vertical resolution such that Direction-of-Arrival responses can be overlaid as a 2D heatmap [34] on the front camera image. In Figure 3 we demonstrate some interesting qualitative findings observed while using the vehicle in urban traffic. The examples highlight that this approach can already detect various important acoustic events for autonomous driving in line-of-sight, such as the presence of vehicles and some vulnerable road users (e.g. strollers). Sound sources that are not yet in line-of-sight can also be detected, as Figure 1c illustrated. This observation is the basis for our occluded vehicle detection described in the next section.

### B. Occluded vehicle detection

We now focus on the task of detecting approaching vehicles behind a blind corner, which we formulate as an online classification task. As the ego-vehicle approaches a blind corner, the acoustic measurements made over short time spans should be assigned to one in a set of four classes,  $\mathcal{C} = \{\text{left}, \text{front}, \text{right}, \text{none}\}$ , with the following semantics:

- *left*: an occluded vehicle approaches from the left behind a blind corner (i.e. no direct line-of-sight),
- *right*: similarly, an occluded vehicle approaching behind a blind corner on the right,
- *front*: a vehicle in front in direct line-of-sight,
- *none*: no approaching vehicle in front of ego-vehicle.

This categorization poses a more challenging prospect than only binary ‘car in proximity’ vs. ‘no car’ classification. While we currently disregard a ‘back’ class, which would overlap with ‘front’ due to the symmetries in our prototype array’s current 2D layout, we do require distinguishing where a vehicle is coming from.

Our method classifies Direction-of-Arrival (DoA) patterns obtained from the array through signal processing, which represent the sound intensity for different directions around the vehicle. For occluded objects, the most salient direction is often a reflection on nearby walls, rather than directly towards the approaching target (we will confirm this in Section IV-B). We therefore propose to distinguish direction by training a classifier on the pattern, rather than taking the most prominent direction at face value. An overview of the processing pipeline is shown in Figure 4.

First, the  $M$  synchronized signals are split into temporal windows of fixed duration of  $\delta t$  seconds. To capture low frequency signals well, we typically use  $\delta t = 1$ s, though shorter windows are also feasible (see Experiments). On each signal, a Short-Time Fourier Transform (STFT) is computed with a Hann windowing function, and a frequency bandpass only keeps responses in the  $[f_{min}, f_{max}]$  Hz range.

From the  $M$  STFTs the DoA energy can be computed for any given azimuth angle  $\alpha$  around the vehicle. We use the Steered-Response Power Phase Transform (SRP-PHAT) [23] which, like many DoA algorithms, identifies direction from the temporal offsets in the signals of microphone pairs, as that relates to their relative distance to the source. The Generalized Cross Correlation Phase Transform (GCC-PHAT) is a common measure for the correlation between the signals of a microphone pair  $m1, m2$  with a given delay  $\theta_{m1,m2}$  between them. The SRP-PHAT can be intuitively be understood as a summation of the GCC-PHAT over all microphone pairs [23] in the array, which improves robustness in adverse acoustic environments.

In our application the distance to the sound source is unknown, but expected to be much larger than the array diameter. We therefore [23] perform far-field localization, i.e. the arriving audio waves appear planar rather than spherical. The time-difference of arrival  $\theta_{m1,m2}(\alpha)$  between microphone  $m1, m2$  can then be written as a function [22] of the azimuth angle  $\alpha$ , given the known microphone 3D spatial positions, the sampling frequency, the sound propagation speed  $c$  (we use a default estimate of  $c = 343$ m/s), and



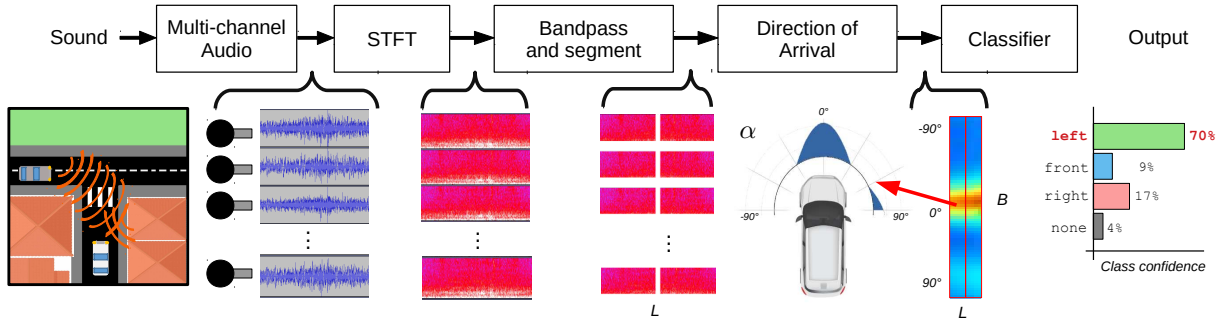


Fig. 4. Overview of our acoustic detection pipeline, see Section III-B for an explanation of the steps.

assuming  $0^\circ$  elevation (i.e. sources lie on horizontal plane).

In practice, we first split the  $M$  STFTs along the temporal dimension into  $L$  non-overlapping segments and per segment compute the DoA energy for multiple azimuth angles  $\alpha$  in front of the vehicle. More segments better capture the temporal changes, but also increase the final feature vector and reduce DoA estimation quality. We distribute the  $[-90^\circ, +90^\circ]$  range into  $B$  equal bins  $\alpha_1, \dots, \alpha_B$ , such that  $\alpha_1 = -90^\circ$  is left of the vehicle, and  $\alpha_{B/2}$  in front. From the original  $M$  signals, we thus obtain  $L$  response vectors  $\mathbf{r}_l = [r(\alpha_1), \dots, r(\alpha_B)]^\top$ , containing the response for  $B$  angles of a segment  $l$ . Finally, these are concatenated to a  $(L \times B)$ -dimensional feature vector  $\mathbf{x} = [\mathbf{r}_1, \dots, \mathbf{r}_L]^\top$ , which is run through a multi-class classifier, e.g. a Support Vector Machine.

To quantitatively evaluate our approach, we shall report (1) the overall accuracy, and (2) the per-class Jaccard index (a.k.a. Intersection-over-Union) as a robust measure of one-vs-all performance. First, for each class  $c$  the True Positives/Negatives ( $TP_c/TN_c$ ), and False Positives/Negatives ( $FP_c/FN_c$ ) are computed, considering target class  $c$  is positive and the other three classes are jointly negative. The overall accuracy is then  $(\sum_{c \in \mathcal{C}} TP_c) / N$  with  $N$  the total number of test samples, and the per-class Jaccard index is,  $J_c = TP_c / (TP_c + FP_c + FN_c)$ .

Our implementation uses a custom ROS node to collect synchronized microphone signals together with other vehicle sensor data. Processing is done in python, using *pyroomacoustics* [22] for acoustic feature extraction, and *scikit-learn* [35] for classifier training.

#### IV. EXPERIMENTS

To validate our method, we created a novel dataset with our acoustic research vehicle in real-world urban environments. As many factors could influence acoustic perception, our experiments are designed to control and study these separately. We recorded at five T-junction locations with blind corners in the inner city of Delft, which we categorize into two types of walled acoustical environments, namely types A and B (see Figure 5). In *static* experiments where the ego-vehicle is not moving, we shall investigate the method's parameters, array size, and generalization across locations. Such static data is easy to collect, and the main source of variance is the approaching vehicle's changing position.

Additional *dynamic* experiments explore generalization to the ego-vehicle driving at  $\sim 15$  km/h.<sup>1</sup>

##### A. Dataset

For the static case, we positioned the ego-vehicle such that the building corners are still visible in the camera and occlude the view onto the intersecting road (on average a distance of  $\sim 7$ -10m from the intersection). We then recorded different types of passing vehicles, though in most recordings the approaching vehicle was a Škoda Fabia 1.2 TSI (2010) driven by us. For the dynamic case, we only made coordinated recordings with the Škoda Fabia to ensure that the encounters were relevant and executed in a safe manner. Scenarios with *left/right/none* approaching vehicles were performed in arbitrary order to prevent undesirable acoustic correlation with background noise to some classes. In  $\sim 19.5\%$  of the recordings the ego-vehicle's noisy internal combustion engine was running to charge its battery.

a) *Sample extraction*: For each recording with an approaching target vehicle, we manually annotate the time  $t_0$  as the moment when the approaching vehicle enters direct line-of-sight. Since the precision of our  $t_0$  estimate is bound the ego-vehicle's camera frame rate (10 Hz), we conservatively regard the last image *before* the incoming vehicle is visible as  $t_0$ . Thus, there is no line-of-sight at  $t \leq t_0$ , and we regard the vehicle visible at  $t > t_0$  (even though it might

<sup>1</sup>Please see animated results in supplementary video.

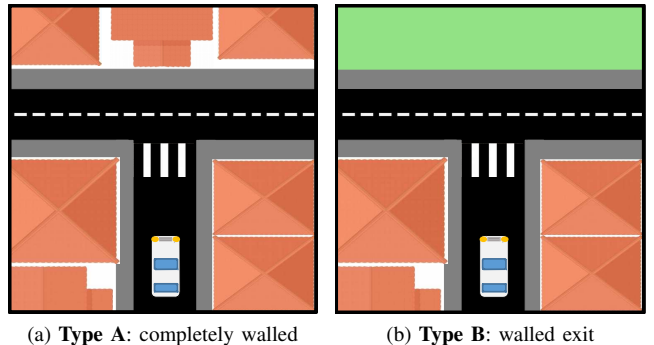


Fig. 5. Schematic of the two considered environment types. The ego-vehicle with microphones approaches the junction from the bottom. Another vehicle might approach behind the left or right blind corner.

TABLE I

SAMPLES PER SUBSET. IN THE ID, S/D INDICATES STATIC/DRIVING EGO-VEHICLE, A/B THE ENVIRONMENT TYPE (SEE FIGURE 5).

ID	Name	left	front	right	none	Sum
SA1	Annaboogerd	14	30	16	30	90
SA2	Kwekerij	22	41	19	49	131
SB1	WillemDreeslaan	17	41	24	32	114
SB2	Vermeerstraat	28	55	27	43	153
SB3	Geerboogerd	22	45	23	45	135
DA	Kwekerij	7	15	8	13	43
DB	Vermeerstraat	10	21	11	22	64
SAB	<i>Total static</i>	103	212	109	199	623
DAB	<i>Total dynamic</i>	17	36	19	35	107
	<i>Total</i>	120	248	128	234	730

only be a fraction of the body). From the recordings we extract short audio samples of  $\delta t$  seconds for our dataset (typically  $\delta t = 1s$ , see Experiments). Let  $t_e$ , the end of the time window  $[t_e - \delta t, t_e]$ , denote a sample’s time stamp at which a prediction could be made. For recordings of the `left` and `right` class, we extract samples at  $t_e = t_0$  with the corresponding class label, and we also extract a sample for the `front` class at  $t_e = t_0 + 1.5s$ . Samples for the `none` class were from recordings with no approaching vehicles. Table I lists statistics of the number of samples per class in our dataset at each recording location.

b) *Data augmentation*: Table I shows that the data acquisition scheme produced imbalanced class ratios, with about half the samples for `left`, `right` compared to `front` and `none`. Our experiments therefore explore *data augmentation* for training. By exploiting the symmetry of the angular DoA bins, augmentation will double the `right` and `left` class samples by reversing the azimuth bin order in all  $r_l$ , resulting in new features with the opposite label, i.e. as if we collected additional data at mirrored locations.

### B. Impact of classifier, features, and training

We first investigate the overall system performance on all Static data from both type A and B locations (i.e. ‘SAB’) using 5-fold cross-validation. The folds on the SAB training data were fixed once for all experiments, with the training samples of each class equally distributed among folds.

We fixed the frequency range to  $f_{min} = 50Hz$ ,  $f_{max} = 1500Hz$ , and the number of azimuth bins to  $B = 30$  (Section III-B), but tested two efficient and robust classifiers, namely a linear Support Vector Machine (SVM) with  $l2$ -regularization weighted by hyperparameter  $\lambda$ , and a non-linear classifier Random Forest (RF) classifier with  $n$  trees. We also varied with the sample length ( $\delta t \in \{0.5s, 1s\}$ ), the DoA algorithm (SRP-PHAT vs MUSIC), the segment count ( $L \in \{1, 2, 3, 4\}$ ), and disabling data augmentation.

Our final choice and reference was the SVM with  $\lambda = 1$ ,  $\delta t = 1s$ ,  $L = 2$ , SRP-PHAT features and data augmentation. Table II shows the results of an ablation study to these parameter choices, and the impact of changing our choices. We note that without data augmentation, and with  $L =$

TABLE II

ABLATION STUDY W.R.T. OUR REFERENCE CONFIGURATION: SVM  $\lambda = 1$ , SRP-PHAT FEATURES,  $\delta t = 1$ ,  $L = 2$ , DATA AUGMENTATION.

Run	Accuracy	$J_{left}$	$J_{front}$	$J_{right}$	$J_{none}$
<i>ours (reference)</i>	<b>0.92</b>	0.79	0.89	<b>0.87</b>	<b>0.83</b>
<i>ours</i> wo. data augment.	<b>0.92</b>	0.75	0.91	0.78	<b>0.83</b>
<i>ours</i> w. MUSIC feat.	0.85	0.63	0.83	0.67	0.70
<i>ours</i> w. $\delta t = 0.5s$	0.91	0.75	0.89	<b>0.87</b>	0.82
<i>ours</i> w. $L = 1$	0.86	0.64	0.87	0.73	0.79
<i>ours</i> w. $L = 3$	<b>0.92</b>	0.74	<b>0.92</b>	0.82	0.81
<i>ours</i> w. $L = 4$	0.90	0.72	0.90	0.77	<b>0.83</b>
<i>ours</i> w. SVM $\lambda = 0.1$	0.91	0.78	0.89	0.81	0.82
<i>ours</i> w. SVM $\lambda = 10$	0.91	<b>0.81</b>	0.86	0.84	<b>0.83</b>
<i>ours</i> w. RF $n = 10$	0.89	0.67	0.88	0.78	0.79
<i>ours</i> w. RF $n = 100$	0.91	0.75	0.91	0.81	0.81
DoA-only [5], [6]	0.63	0.11	0.83	0.28	-

3 segments, overall similar accuracy is achieved, but our reference choices perform better on `left` and `right`. The overall accuracy of the classifiers and hyperparameters on all these choices is similar, though SVM  $\lambda = 1$  has a slight advantage. More importantly, it performs well on both `left` and `right`, so we keep the reference parameters as our main method for all future experiments.

We also illustrate the inherent difficulty of the localization task by comparing to a DoA-only baseline, which was sufficient for past line-of-sight detection methods [5], [6]. The baseline simply selects the strongest DoA azimuth angle  $\alpha$  from the feature  $\mathbf{x}$ , and assigns class `left` iff  $\alpha < -30^\circ$ , `front` iff  $-30^\circ \leq \alpha \leq +30^\circ$  (camera field of view), and `right` iff  $\alpha > +30^\circ$ . We evaluate the baseline on the easier task of only separating these three classes, and ignore the `none` class. The bottom row of Table II confirms that classification must consider reflections, and highlights the benefit of our data-driven approach.

### C. Generalization across acoustic environments

Training and testing on the samples from the same locations provides decent performance as seen in section IV-B. It is interesting to know whether these results generally hold for static experiments, are specific to the locations or whether locations can be categorized in similar environments. To this end, we choose combinations of the training and test sets which do not comprise recordings from the same location.

In Table III, combinations of training and test sets are listed with the corresponding performance of the linear SVM classifier chosen in Section IV-B. The results in the table show a general trend that testing in environments type SA than on type SB environments achieves lower overall accuracy. In particular, some combinations are unsuited for predictions of the `left/right`, such as the ones testing on SA or SA1. Environment B has generally better test performance. This is most prominent at location SB1, where the classifier still performs well on all classes. Interestingly, training on type SA and testing on SB also works well, although with some cutbacks in the `left/right` classes.

We conclude that the classifier cannot generalize easily

TABLE III  
GENERALIZATION ACROSS LOCATIONS AND ENVIRONMENTS.

Test	Training	Accuracy	$J_{\text{left}}$	$J_{\text{front}}$	$J_{\text{right}}$	$J_{\text{none}}$
SA1	SA2	0.66	0.19	0.65	0.00	0.77
SA2	SA1	0.66	0.47	0.12	0.49	0.85
SA	SB	0.67	0.03	0.71	0.09	0.61
SB1	SB23	<b>0.96</b>	<b>0.84</b>	<b>0.95</b>	<b>0.88</b>	<b>0.94</b>
SB2	SB13	0.71	0.69	0.54	0.63	0.42
SB3	SB12	0.76	0.71	0.68	0.65	0.49
SB	SA	0.79	0.41	0.83	0.61	0.67

from one location to another. The classifier may still work at some locations, despite never seeing any sample from this location before. It also does not seem to matter if the training data is from the same environment type or not, though *testing* on environment type B is easier than type A. One explanation might be that the classifier needs to account for location specific reverberation of the ego-vehicle, which may be more pronounced at the front wall of type A environments. We still only have few locations though, future data collection should close the gap between train and test environments.

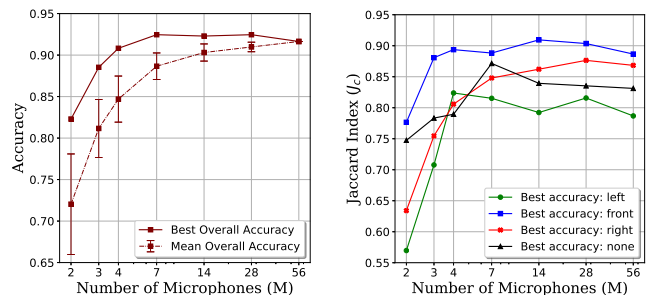
#### D. Impact of number of microphones

We also investigate the impact of the number of microphones  $M$  used, a key benefit of having a large 56 microphone array. Finding an optimal microphone placement is a challenging problem, [36], hence, for a subset of  $M$  microphones, we simply sample 100 random microphone configurations out of the  $\binom{56}{M}$  possibilities from the array and investigate our method using their measurements only. We expect that the overall accuracy would improve with increasing number of microphones, Figure 6a shows that the maximum accuracy already plateaus at around  $M = 7$ . Interestingly, it is possible to use only few microphones, though only 3, as in [6], is too limited for our task. Figure 6b shows the per-class Jaccard indices for the best performing configurations. We find that especially *left* and *right* performance depends on the microphone count, which is expected as differentiation of these cases requires additional directional resolution. Another benefit is that the classification pipeline is faster with fewer computations on audio streams (0.24/0.14/0.04s for  $M = 56/28/14$  in our unoptimized implementation), which is valuable for a low-power implementation on a vehicle.

#### E. Generalization across predictive horizons

Next we investigate the online performance of the method when the approaching vehicle is still further away or has already passed, i.e. at different test times w.r.t  $t_0$ . Additionally, we assess the impact of having more training samples with more varied time stamps  $t_e$ , as till now all *left* and *right* samples were taken from  $t_e = t_0$  only (see Section IV-A).

For this experiment, we first divide static recordings into a fixed train (527 recordings) and test (96 recordings) split. On the training data, we consider default sample extraction method *single sample*, as only one *left* or *right* sample is extracted from their recordings. We also consider



(a) Best and Mean Overall Accuracy (b) Class performance for best layout

Fig. 6. Effect of using randomly sampled subsets of microphones.

augmented *multi sample* extraction, which selects 3 *left* or *right* samples from each recording, namely at  $t_e \in \{t_0, t_0 - 0.5s, t_0 - 1s\}$ . The *front* and *none* samples remain unchanged. For both extraction methods we train our method (as before, an SVM with  $\delta t = 1s$  and  $L = 2$ ), and test the classifier on a sliding window across the 96 test recordings.

Figure 7 shows for both extraction methods the per-class probabilities as a function of test sample time  $t_e$ , grouped by the ground truth label (columns). The SVM class probabilities are obtained with the method in [37]. For example, in Figure 7a the probabilities for *left* using *single sample* show that the model initially predicts on average that no vehicle is approaching. Towards  $t_0$ , the *none* class becomes less likely and the model increasingly favors the correct *left* class. A short time after  $t_0$ , the prediction flips to the *front* class and switches to *right* after the vehicle passed. Similar (mirrored) behavior is observed for vehicles approaching from the right in Figure 7b. The *none* class is constantly predicted as likeliest when no vehicle approached, see Figure 7c. Overall, the prediction matches the events of the recorded scenarios remarkably well. Still, we note that the *left* and *right* classes are only detected when the approaching vehicle is already nearly in line-of-sight, which corresponds to the time of the used training samples with *single sample* extraction.

If we consider the results of using augmented *multi sample* training data (bottom row, Figures 7a-7c), we find that the model is able to predict the correct class earlier than *single sample*, e.g. for *right* at about  $t_e - t_0 = -2.5s$  compared to  $t_e - t_0 = -0.5s$ . This shows that the discriminative acoustic patterns are not limited to the last second before  $t_0$ , but that detection horizon can improve with more varied training data. On average, the method can correctly detect approaching vehicles from sound 2.25 seconds before it is visible, under our experimental conditions.

#### F. Impact of moving ego-vehicle

In our final experiment we investigate the impact of a moving ego-vehicle using the dynamic data recordings.

We follow a similar procedure as the previous experiment to assess the performance, using *multi sample* training data to tackle the variance in the dynamic encounters, but now train our models on all the static samples of environments A

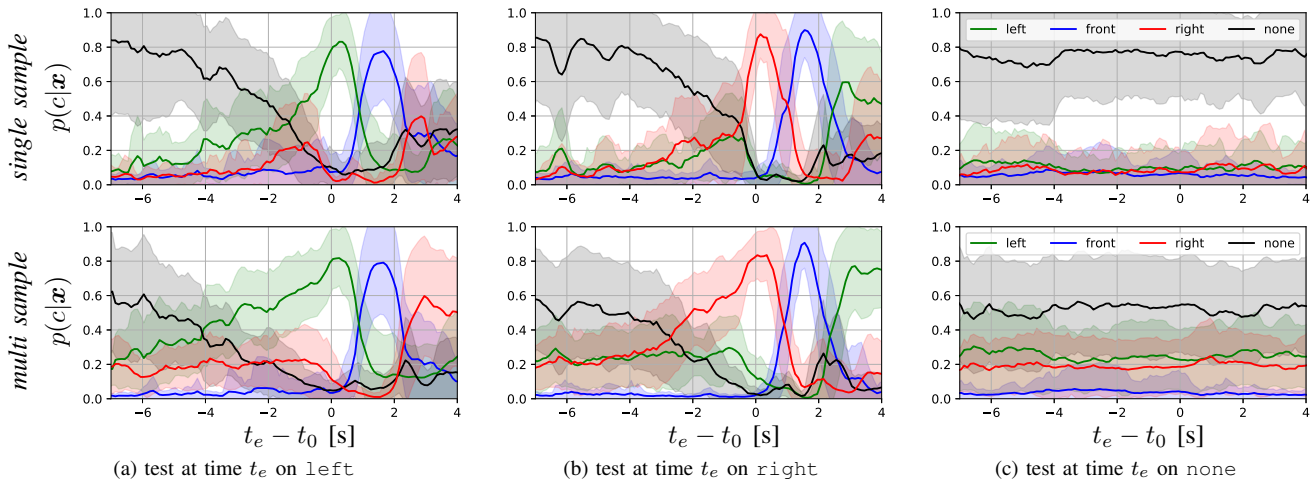


Fig. 7. Mean and std.dev. of per-class probability at different test times. **Top row:** *single sample* training data; **Bottom row:** *multi sample* training data.

and B (SAB). To compare our results across locations, we manually annotate the time  $\tau_0$ , the moment when the ego-vehicle is at the same position as in the static recordings. We align all dynamic recordings to that time as it represents the moment where the ego-vehicle should make a classification decision, irrespective if an approaching vehicle is about to enter line-of-sight ( $t_0$ ) or still further away.

Figure 8 reports the average predicted probability over time for a type A (top row) and B (bottom row) environments. For the type A, the classifier on average correctly predicts *left* and *right* samples, and also shows the favorable tendency for the *none*, around  $t_e = \tau_0$  to  $t_e = \tau_0 + 0.5s$  where the ego-vehicle is closest to the position of the static training data. Unfortunately, for type B the model trained on static data does not work on the dynamic case.

To better understand the differences between the static and dynamic data, we compare in Figure 9a the DoA features of the *left* and *right* recordings averaged over all samples. The figure also shows for type A the development of the DoA over time with respect to  $t_0/\tau_0$  for the static/dynamic case. In the static recordings we see at  $t_0 + 1s$  the prominent band as the vehicle passes in front, but in the seconds before  $t_0$  there is a stronger reflection from the opposite direction, a reflection. In the dynamic case, we see that directional peaks are less pronounced, which we expect is due to non-directional noise of the moving ego-vehicle. Furthermore, the changing ego-perspective results in a switching reflection pattern. Still, around  $\tau_0$  when the ego-vehicle is closest to the static recording location, the DoA features are similar for both classes to their static counterparts, as Figure 9b confirms. For the type B recordings, the DoA comparison Figure 9c shows that the dynamic pattern became less pronounced, and the class difference at  $+60^\circ$  disappeared possibly due to a closer surface reflecting ego-vehicle noise. Training on data with these acoustic ego-motion patterns might reduce the observed performance gap.

## V. CONCLUSIONS

We conclude that a vehicle mounted microphone array can be used to acoustically detect approaching vehicles behind blind corners, and may in the future also serve other acoustic sensing tasks. We found that our configuration using 56 microphones achieved an accuracy of 92% on our 4-class hidden car detection task for a static ego-vehicle. In our experimental setup, we are able to detect an approaching vehicle and predict its direction on average 2.25 seconds before the vehicle becomes visible. Furthermore, the findings of our stochastic array layout search show that good performance can already be achieved with only 7 microphones. Existing efficient DoA techniques can identify nearby objects in direct line-of-sight, otherwise reflection is the main source of information. This necessitates that the local geometry should be taken into account. When the ego-vehicle is moving, the detector trained on static training data still distinguishes *left/right* on one location, but suffers from this domain shift on the other. We are encouraged by our initial findings, though more experimentation is needed as we still used limited data and controlled conditions. Future work will focus on acquiring more training data to improve robustness across locations and enable classification of multiple simultaneous sources.

## REFERENCES

- [1] C. G. Keller, T. Dang, H. Fritz, A. Joos, C. Rabe, and D. M. Gavrila, "Active pedestrian safety by automatic braking and evasive steering," *IEEE T-ITS*, vol. 12, no. 4, pp. 1292–1304, 2011.
- [2] Z. MacHardy, A. Khan, K. Obana, and S. Iwashina, "V2X access technologies: Regulation, research, and remaining challenges," *IEEE Comm. Surveys & Tutorials*, vol. 20, no. 3, pp. 1858–1877, 2018.
- [3] J. K. Suhr and H. G. Jung, "Sensor fusion-based vacant parking slot detection and tracking," *IEEE T-ITS*, vol. 15, no. 1, pp. 21–36, 2013.
- [4] A. Stelling-Kończak, M. Hagenzieker, and B. V. Wee, "Traffic sounds and cycling safety: The use of electronic devices by cyclists and the quietness of hybrid and electric cars," *Transport Reviews*, vol. 35, no. 4, pp. 422–444, 2015.
- [5] M. Mizumachi, A. Kaminuma, N. Ono, and S. Ando, "Robust sensing of approaching vehicles relying on acoustic cues," *Sensors*, vol. 14, no. 6, pp. 9546–9561, 2014.



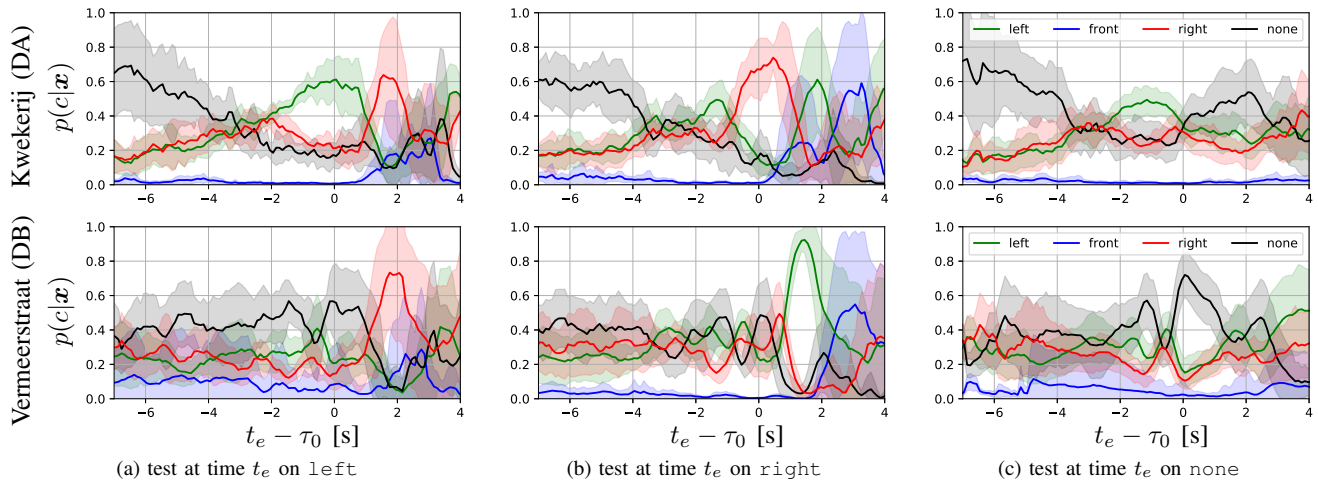


Fig. 8. Mean and std.dev. of predicted class probs. at different times  $t_e$  on *dynamic* recordings with ego-motion, after training on *static* data without ego-motion. Vehicle reached location of training data when  $t_e - \tau_0 = 0$ . **Top row:** at Type A environment. **Bottom row:** at Type B environment.

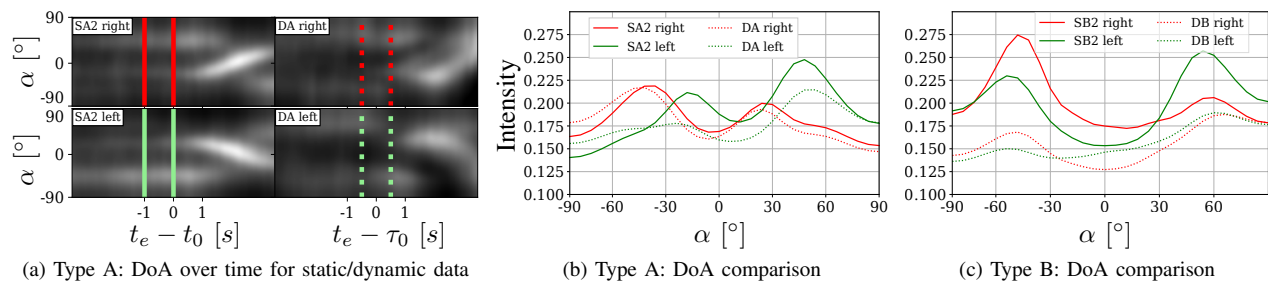


Fig. 9. (a) Average evolution of DoA features over time at Type A location, 1st column for static data (SA), 2nd for dynamic (DA). Intensity indicates DoA energy for azimuth  $\alpha$ . Colors mark 1s at  $t_0$  (static) and around  $\tau_0$  (dynamic). (b) DoA for type A at the marked periods. (c) Similarly for type B.

- [6] Y. Jang, J. Kim, and J. Kim, “The development of the vehicle sound source localization system,” in *APSIPA*. IEEE, 2015, pp. 1241–1244.
- [7] A. V. Padmanabhan, H. Ravichandran, *et al.*, “Acoustics based vehicle environmental information,” SAE, Tech. Rep., 2014.
- [8] K. Asahi, H. Banno, O. Yamamoto, A. Ogawa, and K. Yamada, “Development and evaluation of a scheme for detecting multiple approaching vehicles through acoustic sensing,” in *2011 IEEE Intelligent Vehicles Symposium (IV)*. IEEE, 2011, pp. 119–123.
- [9] V. Singh, K. E. Knisely, S. H. Yönak, K. Grosh, and D. R. Dowling, “Non-line-of-sight sound source localization using matched-field processing,” *The Journal of the Acoustical Society of America*, vol. 131, no. 1, pp. 292–302, 2012.
- [10] T. Toyoda, N. Ono, S. Miyabe, T. Yamada, and S. Makino, “Traffic monitoring with ad-hoc microphone array,” in *Int. Workshop on Acoustic Signal Enhancement*. IEEE, 2014, pp. 318–322.
- [11] S. Ishida, J. Kajimura, M. Uchino, S. Tagashira, and A. Fukuda, “SAVeD: Acoustic vehicle detector with speed estimation capable of sequential vehicle detection,” in *ITSC*. IEEE, 2018, pp. 906–912.
- [12] U. Sandberg, L. Goubert, and P. Mioduszewski, “Are vehicles driven in electric mode so quiet that they need acoustic warning signals,” in *Int. Congress on Acoustics*, 2010.
- [13] L. M. Iversen and R. S. H. Skov, “Measurement of noise from electrical vehicles and internal combustion engine vehicles under urban driving conditions,” *Euronoise*, 2015.
- [14] R. Robart, E. Parizet, J.-C. Chamard, *et al.*, “eVADER: A perceptual approach to finding minimum warning sound requirements for quiet cars,” in *AIA-DAGA 2013 Conference on Acoustics*, 2013.
- [15] S. K. Lee, S. M. Lee, T. Shin, and M. Han, “Objective evaluation of the sound quality of the warning sound of electric vehicles with a consideration of the masking effect: Annoyance and detectability,” *Int. Journal of Automotive Tech.*, vol. 18, no. 4, pp. 699–705, 2017.
- [16] M. Crocco, M. Cristani, A. Trucco, and V. Murino, “Audio surveillance: A systematic review,” *ACM Computing Surveys (CSUR)*, vol. 48, no. 4, pp. 1–46, 2016.
- [17] C. Rascon and I. Meza, “Localization of sound sources in robotics: A review,” *Robotics & Autonomous Systems*, vol. 96, pp. 184–210, 2017.
- [18] L. Wang and A. Cavallaro, “Acoustic sensing from a multi-rotor drone,” *IEEE Sensors Journal*, vol. 18, no. 11, pp. 4570–4582, 2018.
- [19] W. He, P. Motlicek, and J.-M. Odobez, “Deep neural networks for multiple speaker detection and localization,” in *ICRA*. IEEE, 2018, pp. 74–79.
- [20] K. Okutani, T. Yoshida, K. Nakamura, and K. Nakadai, “Outdoor auditory scene analysis using a moving microphone array embedded in a quadcopter,” in *IEEE/RSJ IROS*. IEEE, 2012, pp. 3288–3293.
- [21] I. An, M. Son, D. Manocha, and S.-e. Yoon, “Reflection-aware sound source localization,” in *ICRA*. IEEE, 2018, pp. 66–73.
- [22] R. Scheibler, E. Bezzam, and I. Dokmanić, “Pyroomacoustics: A python package for audio room simulation and array processing algorithms,” in *ICASSP*. IEEE, 2018, pp. 351–355.
- [23] J. H. DiBiase, *A high-accuracy, low-latency technique for talker localization in reverberant environments using microphone arrays*. Brown University Providence, RI, 2000.
- [24] R. Schmidt, “Multiple emitter location and signal parameter estimation,” *IEEE Trans. on Antennas & Propagation*, vol. 34, no. 3, pp. 276–280, 1986.
- [25] M. Hornikx and J. Forssén, “Modelling of sound propagation to three-dimensional urban courtyards using the extended Fourier pstd method,” *Applied Acoustics*, vol. 72, no. 9, pp. 665–676, 2011.
- [26] W. Zhang, P. N. Samarasinghe, H. Chen, and T. D. Abhayapala, “Surround by sound: A review of spatial audio recording and reproduction,” *Applied Sciences*, vol. 7, no. 5, p. 532, 2017.
- [27] K. Osako, Y. Mitsufuji, R. Singh, and B. Raj, “Supervised monaural source separation based on autoencoders,” in *ICASSP*. IEEE, 2017, pp. 11–15.



- [28] A. Saxena and A. Y. Ng, "Learning sound location from a single microphone," in *ICRA*. IEEE, 2009, pp. 1737–1742.
- [29] J. Salamon and J. P. Bello, "Deep convolutional neural networks and data augmentation for environmental sound classification," *IEEE Signal Processing Letters*, vol. 24, no. 3, pp. 279–283, 2017.
- [30] A. Valada, L. Spinello, and W. Burgard, "Deep feature learning for acoustics-based terrain classification," in *Robotics Research*. Springer, 2018, pp. 21–37.
- [31] J. Shen, R. Pang, R. J. Weiss, M. Schuster, N. Jaitly, Z. Yang, *et al.*, "Natural tts synthesis by conditioning wavenet on mel spectrogram predictions," in *ICASSP*. IEEE, 2018, pp. 4779–4783.
- [32] N. Scheiner, F. Kraus, F. Wei, B. Phan, F. Mannan, N. Appenrodt, W. Ritter, J. Dickmann, K. Dietmayer, B. Sick, *et al.*, "Seeing around street corners: Non-line-of-sight detection and tracking in-the-wild using doppler radar," in *Proceedings of the IEEE/CVF Conference on Computer Vision and Pattern Recognition*, 2020, pp. 2068–2077.
- [33] L. Ferranti, B. Brito, E. Pool, Y. Zheng, *et al.*, "SafeVRU: A research platform for the interaction of self-driving vehicles with vulnerable road users," in *Intel. Vehicles (IVS)*. IEEE, 2019, pp. 1660–1666.
- [34] E. Sarradj and G. Herold, "A python framework for microphone array data processing," *Applied Acoustics*, vol. 116, pp. 50–58, 2017.
- [35] F. Pedregosa, G. Varoquaux, A. Gramfort, *et al.*, "Scikit-learn: Machine learning in python," *JMLR*, vol. 12, no. Oct, pp. 2825–2830, 2011.
- [36] A. Malgouzar, M. Snellen, P. Sijtsma, and D. Simons, "Improving beamforming by optimization of acoustic array microphone positions," in *Proc. of the 6th Berlin Beamforming Conference*, 2016, pp. 1–24.
- [37] T.-F. Wu, C.-J. Lin, and R. C. Weng, "Probability estimates for multi-class classification by pairwise coupling," *Journal of Machine Learning Research*, vol. 5, no. Aug, pp. 975–1005, 2004.